solar cycle dependence of the solar wind dynamics: Pioneer, Voyager, and Ulysses from 1 to 5 AU

J. Américo González-Esparza and Edward J. Smith

Jet Propulsion Laboratory, California Institute of Technology, Pasadena, California

Received _ -. ---- ----- _. : accepted

To be submitted to the *Journal of Geophysical Research - Space Physics*, April, 1996.

Short title: GONZÁLEZ-ESPARZA AND SMITH: SOLAR CYCLE AND SOLAR WIND DYNAMICS: 1-5 AU

Abstract. Significant differences between Pioneer and Voyager observations were found in solar wind structure between 1 to 1 AU. These disagreements were attributed to temporal effects related to the solar cycle but no unifying study of Pioneer- Voyager observations was performed. On the basis of maps of large-scale features, we unified and compared observations of solar wind streams, interplanetary shock waves, interaction regions, and magnetic sectors by five spacecraft that traveled from Earth to Jupiter at different phases of the solar sunspot cycle: Pioneer 10 and 11 (declining phase of cycle 20); voyager 1 and 2 (ascending phase of cycle 21); and Ulysses (just after solar maximum 22). We found that solar wind dynamics has a very irregular behavior throughout the solar cycle. There were continual transitions between periods of a few solar rotations dominated by slow solar wind transient events, and irregular patterns of magnetic sectors; and periods of a few solar rotations dominated by interaction regions and well-defined magnetic sectors. These transitions occurred at higher temporal scales, of the order of 2-4 solar rotations. That is the expected slow temporal evolution of coronal holes and current sheet with the solar cycle. It is suggested that these variations are associated with changes in coronal holes and might be related to the early variations of solar wind speed. The differences between Voyager and Pioneer observations were caused by these variations of solar wind dynamics. The pattern of solar wind streams is more stable during the advanced descending phase of the solar cycle (Pioneer 11). In the five spacecraft's observations there were on average, about 3 to 4 interplanetary shocks per solar rotation period. We found a significant population of transient shocks in the outer heliosphere (1–5 AU), in fact, between 40 to 55 percent of the total number

of shocks detected by Pioneer 10, Voyager 1 and 2, and Ulysses were transient forward shocks. However, the shock population changes with the solar cycle and 90 percent of the total number of shocks detected by Pioneer 11 were caused by interaction regions. When slow solar wind is followed by a well-defined stream of corotating fast solar wind, interaction regions are present as early as at about 1 AU. The expansion rate of the interaction regions between 1 to 5 AU is about 94 km/s. Voyager detected, on average, higher flux densities than Pioneer and Ulysses, however, the dynamic pressures detected by the five spacecraft were very similar.

1. Introduction

When Pioneer (10 and 11) [*Smith and Wolfe*, 1976; *Smith and Wolfe*, 1977] and Voyager (1 and 2) [*Gazis and Lazarus*, 1983; *Burlaga et al.* 1984] traveled from Earth to Jupiter, significant differences were found in solar wind structure. The first interplanetary shocks and interaction regions detected by the two missions were reported at different heliocentric distances. On the basis of the analysis on their respective data, the two missions gave different expansion rates of the interaction regions with heliocentric distance. These disagreements have been attributed to temporal effects associated with the solar cycle [*Burlaga*, 1984; *Smith*, 1985]. However, no unifying study of the Pioneer-Voyager observations was carried out.

The aim of this work is to unify and discuss the observations by three different interplanetary missions from Earth to Jupiter at different phases of the solar sunspot cycle: Pioneer, Voyager, and Ulysses. How does the solar wind dynamics between 1 to 5 AU change with the solar cycle? Table 1 shows the schedule of the three missions organized with respect to phases of the solar cycle: Voyager 2 and 1 in the ascending phase of cycle 21, Ulysses just after solar maximum 22, and Pioneer 10 and 11 in the declining phase of cycle 20. The five spacecraft covered the trajectory with different radial speeds and their journeys lasted between 16 and 23 months. Figure 1 shows the last three solar sunspot cycles as reported by the *NOAA Solar Geophysical DATA* and the periods of the spacecraft's trajectories (-10, -11, slow regions).

The solar cycle has a global effect on the heliosphere. The dynamics of the solar

wind is dominated by corotating solar wind streams and transient events. We will briefly review the evolution of the magnetic coronal structure, heliospheric current sheet (HCS), solar wind streams, and CMEs with the solar cycle.

Coronal Structure. The slow temporal evolution of the coronal structure during the solar cycle is summarized in Table 2. The second column describes the evolution of the coronal holes as described by *Hundhausen et al.* [1981] on the basis of the synoptic maps of white light corona during solar cycle 20, and the third column describes the evolution of the current sheet as described by *Hoeksema* [1986] on the basis of the Wilcox maps of solar cycle 21 (see *Hoeksema et al.* [1983], *Hoeksema [1986]* and references therein). The size and location of coronal holes and the shape of the current sheet change with the solar cycle. These variations affect the dynamics of the solar wind. The large equatorial extension of the polar holes and the sinusoidal shape of the current sheet during the descending phase of the cycle (Table 2) are produced by a 'tilt' geometry, where the solar rotational axis and the solar magnetic axis (simplified as a dipole) form a tilt angle that decreases as the cycle approaches minimum (see, e.g., *Hundhausen* [1977], *Zhao and Hundhausen* [1981], and *Mikolov et al.* [1990]).

Smith [1990] suggested that the 'pseudo inclination' or 'tilt' angle of the current sheet can be used to describe the simplified evolution of the current sheet through the solar cycle. This tilt angle is the average value of the maximum north and south latitudinal extensions of the current sheet for each Wilcox map. Close to solar minimum the tilt angle is very small (< 10°). In the ascending phase the tilt angle gradually increases, to the solar maximum the angle is very large (≥ 70°), and in the descending

phase the tilt angle began to decrease to reach a minimum value at about the solar minimum [*Smith*, 1990; *Valdés and Otaola* 1996]. During Voyager observations the tilt angle was increasing rapidly from about 20° to the maximum value in the Wilcox maps ($\geq 70°$) at the time of the Jupiter encounter. During Ulysses observations the tilt angle was decreasing rapidly from the maximum value ($\sim 70°$) to about 40° at the time of the Jupiter encounter (see, e.g., Figure 1 in *Valdés and Otaola*, 1996]). During Pioneer observations there are no Wilcox maps available, but presumably the tilt angle was decreasing from about 60° - 50° to a small angle less than 20°.

HCS and Magnetic Sectors. The evolution of the HCS is associated with the evolution of the current sheet described in Table 2. As the most significant changes of the current sheet occur at mid and high latitudes, at low latitudes (close to the ecliptic plane) there is not a well-defined evolution of the magnetic sector structure with the solar cycle. Comparing in-situ measurements for an extended period of time by ISEE 3 at 1 AU and Pioneer 11 at about 10 AU, *Smith et al.* [1986] reported that the magnetic sector structure is very stable and neither the evolution of the solar wind nor the occurrence of transient events produces major disruptions of the sector structure. So, we do not expect to find any significant heliocentric or solar cycle effect on the magnetic sector structure detected by the five spacecraft.

Solar Wind Streams. Based on studies of the in-situ measurements during solar cycle 20 [*Gosling et al.*, 1976; *Feldman et al.*, 1978; *Feldman et al.*, 1979], *Crooker* [1983] summarized the changes of the averaged values of in-ecliptic solar wind speed V_{sw} and proton temperature T_p in three phases: (1) in solar maximum V_{sw} and T_p had

medium values, (2) in the declining phase V_{sw} and T_p had maximum values, and (3) in solar minimum V_{sw} and T_p had minimum values.

However, the changes in the pattern of solar wind streams seems to be more complex and recently it has been reported they have long term variations with periods of about one year [*Richardson et al.*, 1994; *Gazis et al.*, 1995; *Gazis*, 1996]. This phenomenon is not related to dynamic processes such as the "filtering" or "damping" of the solar wind's 'fine-scale' structure (structures with durations of the order of a solar rotation or less), which are caused by the evolution and collision of interaction regions and transient events in the outer heliosphere that gradually diminish the speed of the fast solar wind and raise the speed of the slow solar wind (see, e.g., the reviews by *Burlaga* [1984] and *Whang* [1990] and references therein). *Gazis* [1996] reported that the long-term enhancements of solar wind speed prevail to very far heliocentric distances (up to 52 AU) and their periodicity changed in 1986. In solar cycle 21, between 1974 and 1985, these enhancements had a period of about 1 year, but in solar cycle 22, between 1987 and 1994, the period was about 1.3 years.

Solar Activity: CMEs. As transient, forward, interplanetary shocks are associated with coronal mass ejections (CMEs) in the inner heliosphere [*Schewenn,* 1983; *Sheeley et al.,* 1983; *Sheeley et al.*, 1985], it is believed that most of the transient forward shocks are driven by fast, wide, CMEs (see, e.g., *Gosling* [1993] and references therein). During the descending phase and solar minimum CMEs are confined to low solar latitudes around the magnetic equator, however, during the solar maximum CMEs are observed in a wider range of latitudes in a more uniform distribution [*Hundhausen et*

al., 1984; *Howard et al.*, 1985; *Handhausen* 1993]. During solar minimum the CMEs are smaller, slower, less massive, and less energetic [*Howard et al.*, 1986]. The occurrence frequency of CMEs tends to follow the solar sunspot cycle in both amplitude and phase: from about 0.2 CMEs per day ($\sim$ 5.4 CMEs per solar rotation period ($\sim$ 27 days)) close to the solar minimum, to about 2 CMEs per day ($\sim$ 57 CMEs per solar rotation period) close to the solar maximum [*Webb and Howard*, 1994]

1.2. Limitations of this Study. From this review, we can expect differences between the observations by the three missions. However, as we will show it, the evolution of the solar wind dynamics is very irregular. On the other hand, the three sunspot cycles were not equivalent to each other. In Figure 1 the three solar cycles had different shapes and durations: cycle 20 had fewer sunspots at its maximum and lasted about 12 years, cycles 21 and 22 had similar shapes lasting about 9 and 10 years respectively. The relatively short interval of each trajectory with respect to the 11-year solar sunspot cycle period could imply that the solar wind observations by the five spacecraft do not represent necessarily their respective solar cycle phases. Furthermore, perhaps the most important restriction to our study is the "annual" variations in solar wind streams. Some of the differences found in solar wind dynamics are more likely related to these yearly variations than to the solar sunspot cycle.

The outline of the paper is as follows: in section 2 we describe how we identify the different elements of solar wind dynamics: interplanetary shocks; interaction regions, magnetic sectors, and interplanetary counterparts of coronal mass ejections (ICMEs). In section 3 we describe the maps of large scale features of the five spacecraft. In section 4

we discuss the observations and their possible relation with the solar cycle, and section 5 presents our conclusions.

2. Identification of Large-Scale Features

Our study is based on maps of large-scale features in the solar wind. These maps consist of successive rows of 27 days (approximately the solar rotation period as observed by the spacecraft), where polarity of the interplanetary magnetic field (IMF), forward and reverse shock waves, interaction regions, and ICMEs are characterized by different symbols. A comprehensive map of Ulysses large-scale observations has been reported elsewhere [*González-Esparza et al.*, 1996]. To produce similar maps of Pioneer and Voyager observations we obtained plasma and magnetic field data (in one hour averages) from the NSSDC. The maps were generated scanning 27-day plots of: IMF magnitude $|B|$, IMF longitudinal angle ϕ, solar wind speed V_{sw}, proton density N_p and proton temperature T_p (Voyager T_p data were not available at NSSDC). The criteria to identify the large-scale features are described bellow.

Using the plots of ϕ we identified the polarity of the IMF. To consider an abrupt rotation of ϕ ($\Delta\phi \approx 180°$) as a HCS crossing, the new polarity was required to last at least one day and not be related to a transient event. We verified our polarity maps by comparing them with previous reports of Pioneer 10 and 11 observations by *Smith and Wolfe* [1976] and *Smith and Wolfe* [1977] and Voyager 1 and 2 observations by *Burlaga et al.* [1984].

Interaction regions were identified by simultaneously examining 27-day plots of $|B|$,

V_{sw}, N_p, and T_p (when available). An interaction region is characterized by well-known signatures of a fast solar wind stream overtaking a slow solar wind stream, and between these two streams there is a well-defined compression region which contains a distinctive stream interface dividing the two compressed fluids [*Gosling et al.*, 1978]. Interaction regions can be recurrent structures called corotating interaction regions (CIRs) [*Smith and Wolfe,* 1977]. The absence of T_p data in Voyager observations was compensated by the information provided in Figures 11 and 12 by *Burlaga et al.* [1984].

The list of interplanetary shock waves detected by Pioneer 10 and 11 was obtained from *Smith* [*personal communication*] and visual identification using the 27-day plots of $|B|$ and plasma parameters. The list of shock waves detected by Voyager 1 and 2 was obtained from Figures 11 and 12 by *Burlaga et al.* [1984], a shock list of Voyager 1 by P. R. Gazis [*private communication*], and visual identification in the 27-day plots

Unfortunately, the identification of ICME's (ejecta signatures) in in-situ solar wind observations is still, as called by J. T. Gosling [1993], "something of an art". We have not yet found a signature unequivocally associated with ICMEs. Limited by the data available, we attempted to identify ICME s in Pioneer 10 and 11 observations looking for anomalous low T_p and/or magnetic cloud signatures after the passage of transient forward shocks. In the case of Voyager observations, due to the absence of T_p data in the NSSDC files at the time of the study, we used the magnetic clouds identified by *Burlaga et al.* 1984]. As a result, we obtained a poor characterization of the occurrence of ICMEs.

2.1. **Classification of Interplanetary Shocks** Depending on their causes

interplanetary shock waves are classified in two types: corotating shocks (caused by interaction regions) and transient shocks (attributed nominally to ICMEs). Corotating shocks are found leading (forward shock) and/or trailing (reverse shock) interaction regions. Forward transient shocks are associated with post-shock ejecta signatures. The global geometry and spatial extent of transient and corotating shocks is different. As interplanetary shock waves are the strongest perturbations propagating through the heliosphere, and corotating and transient shocks have different characteristics, the shock population is an important parameter to describe the large-scale characteristics of the heliosphere.

3. Maps of Large-Scale Structures

Figure 2 shows solar wind bulk speed V_{sw} against heliocentric distance as observed by the five spacecraft from Earth to Jupiter. The five spacecraft detected different patterns of solar wind streams. Voyager 1 and 2 (top of Figure 2) observed a variable slow wind ($V_{sw} \leq 450\,km/s$) with irregular peaks associated with transient fast wind causing transient interaction regions. In the middle panel, Ulysses observations from 1 to 2.9 AU were characterized by transient events, in particular the large peak in March 1991 at about 2.4 AU, and from 2.9 to 5.4 AU the solar wind was dominated by quasi-stationary fast wind streams producing CIRs. At the bottom of the Figure 2, although launched within one year of one another, Pioneer 10 and 11 observations are quite different with respect to each other. Pioneer 11 detected the simplest pattern of solar wind streams with enormous, quasi-stationary fast wind streams ($V_{sw} \geq 650\,km/s$)

producing an impressive series of ('11. Pioneer 10 detected several temporal variations: from about 2 to 3 AU the fast wind disappeared (August 1972 events), and from 3 to 4.8 AU the solar wind streams were involved in a long-term change with both limits of fast and slow wind gradually raising to a maximum at about 3,63.7 AU and both then decreasing again. This long term change could be associated with the yearly variations referred earlier, in particular, with Figures 4 and 5 reported by *Gazis et al.* [1995]. Note in the five plots of Figure 2, a clear tendency of the slow solar wind to increase in magnitude with heliocentric distance, evidence of the acceleration of the slow solar wind by the following fast wind.

The next subsections discuss the five maps of large scale observations.

3.1. **Voyager 1.** Figure 3 shows the map of large-scale features of Voyager 1. The behavior of the magnetic sectors was regular with some periods with undefined polarity. At the beginning of the trajectory, between .7 and 1.75 AU, Voyager 1 detected four interaction regions, afterwards a change in dynamics produced a series of transient shocks. After the gap in plasma data there were similar changes in dynamics from periods dominated by transient forward shocks to periods dominated by interaction regions. Comparing bottom and top of the figure, there was a clear tendency of interaction regions to increase their duration with heliocentric distance. Presumably there are many more ICME events in these observations. In fact, those periods with undefined magnetic polarity (i.e., ϕ could not be unequivocally associated with either positive or negative Parker's spiral direction), might be associated with the numerous ejecta expected at this phase of the solar cycle, however, we were not able to identify

these ejecta to corroborate this possibility.

3.2. Voyager 2. Figure 4 shows the map of large-scale features of Voyager 2. Similar to the previous figure, the magnetic sector structure was complex and unstable. As we would expect, observations by Voyager 2 and Voyager 1 (Figure 3) are similar to each other, however, there are significant differences: many transient forward shocks were detected by only one Voyager, and, in some cases, the duration of the same interaction region and polarity sectors varies in the two spacecraft (see *Burlaga et al. [1984]* for more details on these observations). From 2.7 to 3.7 AU Voyager 2 observed an extended period dominated by transient forward shocks without interaction regions. In this period fast solar wind streams were absent (Figure 2). Interaction regions appeared again after 3.7 AU. Similar to the previous figure the occurrence rate of ICMEs is too low to what we would expect.

3.3. Ulysses. Figure 5 shows the map of large-scale features of Ulysses in-ecliptic observations. These observations can be broadly divided into two intervals: (1) from 1 to 2.9 AU, dominated by transient forward shocks, and (2) from 2.9 to 5.4 AU, dominated by interaction regions (see *González-Esparza et al.* [1996] for a detailed discussion). The first interval is characterized in Figure 2 by the absence of fast wind and then a large peak ($V_r \geq 900\,km/s$) associated with the series of transient shocks and ICMEs called 'March 1991' events [*Phillips et al.*, 1992] (from day 91:064 to 91:091 in Figure 5). During the first interval the sector structure was complex with alternating four and six magnetic sectors per solar rotation. In the second interval the sector structure was simpler dominated by two magnetic sectors.

3.4. Pioneer 10. Figure 6 shows the map of large-scale features of Pioneer 10. The sector structure was complex and unstable with alternating two, six, and four magnetic sectors per solar rotation. At the bottom of Figure 6, from 1.2 to 2.6 AU, the dynamics was dominated by three interaction regions (one caused by fast wind with positive IMF and two caused by fast wind with negative IMF). From about 2.6 to 3.4 AU there was a change in solar wind streams (Figure 2) and the interaction regions caused by fast wind with negative IMF disappeared. Afterwards, the three interaction regions appeared again. Note the numerous transient forward shocks detected by Pioneer 10 in some solar rotations.

3.5. Pioneer 11. Figure 7 shows the map of large-scale features of Pioneer 11. The first nine solar rotations (from day 73:096 to day 73:339) coincide in time with the last nine solar rotations of the map of Pioneer 10 (Figure 6), however, the comparison between the two maps is complicated by the heliocentric and angular distances separating the two spacecraft. In this map, the magnetic sectors are simple and well-defined. CIRs, produced by fast winds with positive and negative IMF, were continuously detected from 1 AU to the Jupiter flyby. This regularity and simplicity of the large-scale dynamics is not surprising from Figure 2, where corotating high-speed wind overtakes slow wind every solar rotation.

4. Discussion

4.1. Shock Population. Based on the analysis of the maps of large-scale structures Table 3 summarizes the type of shock waves (corotating and transient

spacecraft. The daily averages of V_{sw} are divided into four ranges denoted by different colors: very slow wind ($V_{sw} < 350$ km/s), slow wind (350 km/s $\geq V_{sw} < 450$ km/s), fast wind (450 km/s $\geq V_{sw} < 600$ km/s), and very fast wind ($V_{sw} \geq 600$ km/s). Figure 8 shows several solar rotations absent of fast wind in Voyager, Ulysses, and Pioneer 10 observations (predominant dark gray – gray rows in the maps). In general, these slow wind periods correspond to periods dominated by transient events and complex magnetic sector structures in their corresponding maps of large-scale features. However, when there is a well-defined pattern of quasi-stationary fast wind behind slow wind in a speed map (light gray–white vertical columns surrounded by darker regions in Figure 8), then, in general, there is a period dominated by interaction regions at the same location in the corresponding map of large-scale features.

Figure 8 shows that there are continual variations in the pattern of solar wind streams at all the phases of the solar cycle. These temporal variations should be related to changes of the solar wind sources, suggesting that there are continual variations in the structure of coronal holes at temporal scales of the order of one or a few solar rotations. Further study of these variations in solar streams and coronal holes could corroborate this possibility.

Figure 9 shows the histograms of solar wind bulk speed V_{sw} for the five spacecraft from Earth to Jupiter. The speed distributions present a similar evolution with the solar cycle as previously reported. *Gosling et al.* [1976] studied annual distributions of V_{sw} observed at 1 AU from 1962 to 1974 (cycle 20), and they found that close to solar maximum the mean value of the speed distribution had a minimum value which

tended to increase reaching a maximum value during the descending phase of the cycle. In this study, Voyager 1 has the lowest mean value of the V_{sw} distributions, whereas Pioneer 11 has the highest mean value and the larger standard deviation. This result can be explained by the tilt geometry during the descending phase of the cycle, that causes fast solar wind streams reach higher values and longer duration.

Table 4 shows different solar wind parameters as observed by the five spacecraft. The second column shows the mean bulk speeds values and their standard deviation discussed in Figure 9. The third column shows mean values of proton flux density normalized to 1 AU ($\frac{1}{n}\sum_{i=1}^{n} V_{sw_i} N_{p_i} R_{d_i}^2$) and their standard deviation. Voyager detected, on average, slower but denser solar wind than Pioneer causing that the Voyager's mean flux densities were higher than Pioneer flux density detected by Ulysses was also higher than Pioneer measurements. This result is somehow opposite to the report by *Richardson et al.* [1995] where they found that both flux density and dynamic pressure have a minimum close to the solar maximum. In this case, the flux density was higher in the ascending and post-maximum phases than in the descending phase. The next column of Table 4 shows mean values of the proton dynamic pressure normalized to 1 AU ($\frac{1}{n}\sum_{i=1}^{n} V_{sw_i}^2 N_{p_i} R_{d_i}^2$). In this case the higher speeds detected by Pioneer compensate their lower values of flux densities and Pioneer and Voyager dynamic pressures were very similar. Ulysses detected the highest mean value of dynamic pressure and this result is similar to Figure 5 in *Richardson et al.* [1995] where there are peaks in dynamic pressure after solar maxima. However, we should keep in mind that solar wind properties

just temporal variations.

The last two columns of Table 1 give two parameters of solar wind dynamics: the rate of interplanetary shocks and the rate of interaction regions per solar rotation averaged on the whole trajectory. Voyager 1, Ulysses, and Pioneer 10 observations were similar: they detected on average about one interaction region and 3–4 interplanetary shocks per solar rotation. However, Pioneer 11 and Voyager 2 are very different. The probability of finding interaction regions in Pioneer 11 data is three times higher than in Voyager 2 data. The character of their shock population is contrasting: most of the shocks detected by Voyager 2 were transient, whereas most of the shocks detected by Pioneer 11 were corotating (last column of Table 3).

4.3. Magnetic Sectors. In all the maps of large scale features the behavior of the magnetic sector structure was unstable and their pattern and extension varied continuously. As pointed out in the introduction, these changes are not associated with heliocentric evolution but are temporal. These changes are related to the variations of solar wind speeds (Figure 8) and supports the suggestion that they are associated with variations of the coronal holes.

As pointed out by previous studies there is not a well-defined evolution of the in-ecliptic magnetic sector structure through the solar cycle. In fact, on average, the most complex sector structure (defined by the most fragmented sector structure per solar rotation) was observed by Pioneer 10, and the simplest, on average, was observed by Pioneer 11. A general tendency detected in the five spacecraft was that when the large-scale dynamics was dominated by interaction regions the magnetic sector structure

was simple and well-defined. But when the interaction regions were absent the magnetic sector structure, in general, was complex and unstable.

4.4. Interaction Regions. One of the differences between Pioneer and Voyager results was the estimation of the temporal expansion rate of the interaction regions, i.e., the relatively speed between the forward and the reverse corotating shocks. *Smith and Wolfe* [1977] calculated that interaction regions widen at a rate about 100 km/s, and *Burlaga et al.* [1984] calculated about 180 to 270 km/s. Figure 10 shows the radial extent or wideness W_{cir} (normalized to AU) of all the CIRs observed by the five spacecraft against heliocentric distance. To estimate the W_{cir} of each interaction region we calculated the average solar speed throughout the interaction region and we multiplied it by the temporal duration of the interaction region in the data series ($W_{cir_j} = \bar{V}_{cir_j} \cdot \Delta t_{cir_j}$). We applied a linear fit to the W_{cir} points in Figure 10 and we obtained a wideness rate of about .12 AU per AU. When we applied the same linear fit to the W_{cir} points of each spacecraft separately, we obtained similar slopes values of about 0.2 AU per AU. Although we do not expect a linear formation and evolution of CIRs, this result gives a good approximation to characterize the evolution of interaction regions between 1 to 5 AU. Figure 11 shows the histogram of the average speeds of all the interaction regions in Figure 10. CIRs propagate with a broad range of speeds ($325\ km/s \leq \bar{V}_{cir_j} \leq 675\ km/s$), however, the distribution has a bell shape and the mean value is 470 km/s. We can use these results to estimate the approximated temporal expansion rate of CIRs, that should be: the spatial enlargement of a CIR after

traveling 1 AU divided by the time that takes to the CIR to cross 1 AU

$$\frac{0.2 \times 1\ AU}{1\ AU\ /\ 470\ km\ s^{-1}} = 94\ km\ s^{-1}$$

This result is very close to the value given by *Smith and Wolfe* [1977] on the basis of a very different method (they applied the Rankine-Hugoniot solutions to calculate the propagation speed of the forward and the reverse corotating shocks).

Figures 10 and 11 show a significant diversity in the wideness of CIRs at about the same heliocentric distance, and in their speed propagation. These variations are related to the particular characteristics of the solar wind streams causing the interaction regions.

5. Conclusions

We have studied the observations of five different spacecraft from 1 to 5 AU in order to understand how the solar wind dynamics changes with the solar cycle. We found an irregular evolution characterized by continual variations in the pattern of solar wind streams and magnetic sectors in temporal scales of the order of 2–4 solar rotation periods. These variations caused alternating intervals dominated by slow wind, transient events, and irregular magnetic sectors; and intervals dominated by interaction regions and well-defined magnetic sectors. The differences between Pioneer and Voyager observations were caused by these transitions. The absence of interaction regions in the early part of Voyager [*Gazis and Lazarus*, 1983] and Ulysses [*González-Esparza et al.*, 1996] trajectories was related to periods dominated by slow solar wind. If there

is a well-defined pattern of corotating fast solar wind, interaction regions are present as close as about 1 AU. The distributions of solar wind speed seem to evolve with the solar cycle as previously reported at 1 AU [*Gosling et al.*, 1976], this suggest that during the advanced part of the descending phase the dynamics is more stable, dominated by interaction regions as was detected by Pioneer 11. Only at that phase of the cycle, we can say that most, if not all, interplanetary shocks in the outer heliosphere (1 to 6 AU) are caused by interaction regions.

Acknowledgments. We are grateful to Marcia Neugebauer for reading the manuscript and to Paul R. Gazis who provided his shock list for Voyager 1. The plasma and magnetic field data for this study were obtained from the National Space Science Data Center at Goddard Space Flight Center. The Pioneer 10 and 11 plasma data are from the experiment of J. Wolfe. The Voyager 1 and 2 plasma data are from the experiment of H. Bridge and J. Belcher. The Voyager 1 and 2 magnetic field data are from the experiment of N. Ness. The Ulysses plasma data are from the experiment of J. Phillips. J. A. G-E. is grateful to the National Research Council for financial support as a Resident Research Associated at JPL. The research at Jet Propulsion Laboratory, California Institute of Technology, was supported by the National Aeronautics and Space Administration.

References

Burlaga, L. F., MHD processes in the outer heliosphere, *Space Sci. Rev., 39,* 255-316, 1984.

Burlaga, L. F., L. W. Klein, R. P. Lepping, and K. W. Behannon, Large scale interplanetary magnetic fields: Voyagers 1 and 2 observations between 1 au and 9.5 au. *J. Geophys. Res., 89,* 10659-10668, 1984.

Crooker, N. U., Solar cycle variations of the solar wind, in *Solar Wind Five,* M. Neugebauer, editor, NASA headquarters and JPL, 305-313, 1983.

Feldman, W. C., J. R. Asbridge, S. J. Bame, and J. T. Gosling, Long-term solar variations of selected solar wind properties: Imp 6,7, and 8 results, *J. Geophys. Res., 83,* 2177-2189, 1978.

Feldman, W. C., J. R. Asbridge, S. J. Bame, and J. T. Gosling, Long-term solar wind electron variations between 1971 and 1978, *J. Geophys. Res., 84,* 7371-7377, 1979.

Gazis, P. R., and A. J. Lazarus, The radial evolution of the solar wind, 1 - 10 au, in *Solar Wind Five,* M. Neugebauer, editor, NASA headquarters and JPL, 509-519, 1983.

Gazis, P. R., J. D. Richardson, and K. I. Paularena, Long term periodicity in solar wind velocity during the last three solar cycles, *Geophys. Res. Lett., 22,* 1165-1168, 1995.

Gazis, P. R., Long-term enhancements in solar wind speed, *J. Geophys. Res., 101,* 415-424, 1996.

González-Esparza, J. A., A. Balogh, R. J. Forsyth, M. Neugebauer, E. J. Smith, and J. L. Phillips, Interplanetary shock waves and large-scale structures: Ulysses' observations in and out of the ecliptic plane, *J. Geophys. Res., in press,* 1996.

Gosling, J. T., J. R. Asbridge, S. J. Bame, and W. C. Feldman, Solar wind speed variations: 1962-1974. *J. Geophys. Res., 81,* 5061, 1976.

Gosling, J. T., J. R. Asbridge, S. J. Bame, and W. C. Feldman, Solar wind stream interfaces, *J. Geophys. Res., 83*, 1401-1412, 1978.

Gosling, J. T. , The solar flare myth, *J. Geophys. Res., 98*, 18937-18949, 1993.

Hoeksema, J. T., J. M. Wilcox, and P. H. Scherrer, The structure of the heliospheric current sheet:1978-1982, *J. Geophys. Res. , 88*, 9910-9918, 1983.

Hoeksema, J. T., The relationship of the large-scale solar field to the interplanetary magnetic field: what will ulysses find?, in *The Sun and the Heliosphere in Three-Dimensions*, R. G.Marsden, editor, *D. Reidel Publishing Company*, 241-254, 1986.

Howard, R. A,, N. R. Sheeley, Jr., M. J. Koomen, and D. J. Michels, Coronal mass ejections: 1979-1981, *J. Geophys. Res., 90*, 8173-8191, 1985.

Howard, R. A., N. R. Sheeley, Jr., D. J. Michels, and M. J. Koomen, The solar cycle dependence of coronal mass ejections, in *The Sun and the Heliosphere in Three-Dimensions*, R. G. Marsden, editor, *D. Reidel Publishing Company*, 107-111, 1986.

Hundhausen, A. J., An interplanetary view of coronal holes, in *Coronal Holes and High Speed Streams*, J. B. Zirker, editor, Colorado Associated University Press, Boulder, Colorado, 225-330, 1977.

Hundhausen, A. J., Solar activity and the solar wind, *Rev. of Geophys. and Space Phys., 17*, 2034-2048, 1979.

Hundhausen, A. J., R. T. Hansen, and S. P. Hansen, Coronal evolution during the sunspot cycle: coronal holes observed with the Mauna Loa k-coronameters, *J. Geophys. Res., 86*, 2079-2094, 1981.

Hundhausen, A. J., C. B. Sawyer, L. House, R. M. E. Illing, and W. J. Wagner, Coronal mass ejections observed during the solar maximum: latitude distribution and rate of

occurrence, *J. Geophys. Res.*, *89*, 2639-2646, 1984

Hundhausen, A. J., Sizes and locations of coronal mass ejections: SMM observations from 1980 and *1984-1989*, *J. Geophys Res.*, *98*, 13177-13200, 1993

Mihalov, J. D., A. Barnes, A. J, Hundhausen and E. J. Smith, Solar wind and coronal structure near sunspot minimum: pioneer and smm observations from 1985-1987, *J. Geophys. Res.*, *95*, 8231-8242 1990.

Neugebauer, M,, Large scale and solar cycle variations of the solar wind, *Space Sci. Rev., 17, 221-254, 1975.*

Phillips, J. L., S. J Bame, J. T. Gosling, D. J. McComas, B. E. Goldstein, E. J. Smith, A. Balogh, and R. J. Forsyth, Ulysses plasma observations of coronal mass ejections. *Geophys. Res. Lett., 19,* 1239, 1992

Richardson, J. D., K. I. Paularena, J. W. Belcher, and A. J. Lazarus, Solar wind oscillations with a 1.3-year period, *Geophys. Res. Lett.*, *21*,1559, 1994.

Richardson, J. D., Paularena, K. I., A. J. Lazarus and J. W. Belcher, Radial evolution of the solar wind from IMP 8 to Voyager 2. *Geophys. Res. Lett.*, *22*, 325-328, 1995.

Schewenn, R., Direct correlations between coronal transients and interplanetary shocks. *Space Sci. Rev.*, 34, 83, 1983.

Sheeley, N, R., R. A. Howard, M. J. Koomen, D. J. Michaels, R. Schwenn, K, H. Muhlhauser, and H. Rosenbauer, Association between coronal mass ejections and interplanetary shocks, in *Solar Wind Five,* M. Neugebauer, editor, NASA headquarters and the Jet Propulsion Laboratory, 1983.

Sheeley, N. R., R. A. Howard, M. J. Koomen, D. J. Michaels, R. Schwenn, K. H. Muhlhauser, and H. Rosenbauer, Coronal mass ejections and interplanetary shocks. *J. Geophys. Res.*,

90, 163-190, 1985.

Slavin, J. A., and E. J. Smith, Solar cycle variations in the interplanetary magnetic field, in *Solar Wind Five,* M. Neugebauer, editor, NASA headquarters and JPL, 323-331, 1983.

Smith, E. J., and J. H. Wolfe, Observations of interaction regions and corotating shocks between one and five au. *Geophys. Res. Lett., 3,* 137-140, 1976.

Smith, E. J., and J. H. Wolfe, Pioneer 10, 11 observations of evolving solar wind streams and shocks beyond 1 au, in *Study of Traveling Interplanetary Phenomena/1977,* M. A. Shea, D. F. Smart, and S. T. Wu, editors, D. Reidel, 227-257, 1977.

Smith, E. J., Interplanetary shock phenomena beyond 1 au, in *Collisionless Shocks: Reviews of Current Research,* B. T. Tsurutani and R. G. Stone, editors, *Geophysical Monograph, 35,* 69, 1985.

Smith , E. J., J. A. Slavin, and B. T. Thomas, The heliospheric current sheet: 3-dimensional structure and solar cycle changes, in *The Sun and the Heliosphere in Three-Dimensions,* R. G. Marsden, editor, *D. Reidel Publishing Company,* 267-274, 1986.

Smith, E. J., The heliospheric current sheet and modulation of galactic cosmic rays, *J. Geophys. Res., 95,* 18731-18743, 1990.

Valdés-Galicia, J. F., and J. A. Otaola, The latitudinal structure of the heliospheric current sheet during solar activity cycles 21 and 22, *J. Geophys. Res., 101,* 2475-2483, 1996.

Webb, F. W., and R. A. Howard, The solar cycle variation of coronal mass ejections and the solar wind mass flux, *J. Geophys. Res., 99,* 4201-4220, 1994.

Whang, Y. C., Shocks interactions in the outer heliosphere, *Sp. Sc. Reviews, 53,* 339, 1990.

Zhao, X., and A. J. Hundhausen, Organization of solar Wind plasma properties in a tilted,

heliomagnetic system, *J. Geophys. Res.*, *86*, 5423, 1981

This manuscript was prepared with the AGU LaTeX macros v3.0.

Figure 1. Solar sunspot numbers from 1964 to 1995 as reported by *NOAA Solar Geophysical DATA*. The periods of Pioneer 10 and 11, Voyager 1 and 2, and Ulysses trajectories from the Earth to Jupiter are denoted by dotted lines in the figure. The three missions covered the same heliocentric range at different phases of the solar sunspot cycle.

Figure 2. One hour average of solar wind speed as detected by the five spacecraft from Earth to Jupiter against the heliocentric distance. The five spacecraft detected different patterns of solar wind streams, and there are significant temporal changes in the streams detected by each spacecraft. Pioneer, Voyager and Ulysses data were obtained from the NSSDC.

Figure 3. Map of large-scale features of Voyager 1. Every 27-day row corresponds to an approximate solar rotation observed by the spacecraft. The chronological order is from the bottom to top. Denoted by characteristic symbols are shown: forward shocks (left arrows), reverse shocks (right arrows), CIRs (dark), CMEs (wavy) and the background magnetic sectors (white=positive, gray= negative; light gray= undefined). To produce this map we used information previously reported by *Burlaga et al.* [1984]. See text for discussion.

Figure 4. Map of large-scale features of Voyager 2. This figure has the same format of the previous figure. The time period covered by this map coincides with the time period of the previous figure. To produce this map we used information previously reported by *Burlaga et al.* [1984]. See text for discussion.

Figure 5. Map of large-scale features of Ulysses in-ecliptic observations. This map was previously reported by *González-Esparza et al.* [1996]. See text for discussion.

Figure 6. Map of large-scale features of Pioneer 10 with the same format of the previous figures. See text for discussion.

Figure 7. Map of large-scale features of Pioneer 11 with the same format as of the previous figures. The first nine solar rotations overlap in time the last nine solar rotations of the previous figure. However the comparation of the two maps is difficult due to the heliocentric and angular distance between the two spacecraft.

Figure 8. Maps of daily averages of solar wind speed of the five spacecraft. Every row corresponds to 27 days and the order goes from the bottom to top (similar format than Figures 3-7). Each map covers exactly the same time period than their corresponding map of large-scale features. The daily averages of solar wind speed were divided into four ranges: (1) very slow wind ($V_{sw} < 350$ km/s) (dark gray), (2) slow wind ($350 \leq V_{sw} < 450$ km/s) (gray), (3) fast wind ($450 \leq V_{sw} < 600$ km/s) (light gray), and (4) very fast wind ($600 \leq V_{sw}$ km/s) (white). Data gaps are denoted by black. These maps illuminate the role and variability of the solar wind streams in the solar wind dynamics (see text for discussion). Pioneer Voyager and Ulysses data were obtained from the NSSDC.

Figure 9. Histograms of solar wind speed (1-hour averages) as detected by the five spacecraft from 1 to 5 AU. The shape and evolution of these distributions are in agreement with previous reports of solar wind distributions at different phases of the solar cycle by *Gosling et al.* [1976]. Pioneer, Voyager and Ulysses data were obtained from the NSSDC.

Figure 10. Radial extent or Widenes W_{cir} (normalized to AU) of all the interaction regions detected by the five spacecraft against heliocentric distance. The W_{cir_j} of each CIR was calculated by multiplying the average solar wind speed throughout the CIR V_{cir_j} by its temporal duration Δt_j in the data series. Based on the linear fit of the W_{cir} points, from 1 to 5 AU, interaction regions expand by an approximated rate of about 0.2 AU per AU.

Figure 11. Frequency histogram of the average speed V_{cir} of all the CIRs plotted in Figure 10. Interaction regions propagate with a broad range of V_{cir} between 325-675 km/s,

Table 1. Solar sunspot cycle phase and schedule of the three missions.

	Solar Cycle Phase	Launch	Jupiter Flyby	Duration (in months)
Voyager 2	ascending (21)	2 Aug 1977	Jul 1979	23
Voyager 1	ascending (21)	5 Sep 1977	Mar 1979	18
Ulysses	post-maximum (22)	6 Oct 1990	Feb 1992	16
Pioneer 10	descending (20)	2 Mar 1972	Dec 1973	21
Pioneer 11	descending (20)	5 Apr 1973	Nov 1974	20

Table 2. Involution of the coronal magnetic structure through the solar cycle

solar Cycle	Coronal Holes*	Current Sheet
Ascending phase	polar holes shrank and disappear, but they evolve in a very different way disappearing at different times	the latitudinal extent of the current sheet increases to higher latitudes, disrupting the simple equatorial configuration of the previous minimum
Maximum	no polar holes, but small holes around, but	very complex structure, the main current shed extents almost from pole to pole and , 11 in latitudes small isolated current sheets appear
Descending phase	after the reversal in polarity, polar ol . re h and grow in size with large equatorial extensions	the structure is simpler and the current sheet has a sinusoidal shape extended over a large range of latitudes
Minimum	polar holes have maximum extensions and there are no equatorial holes	the current sheet is very stable lying over the solar equator

* Based on the description by *Hundhausen et al.* [1981]
† Based on the description by *Hoeksema* [1986]

Table 3. Evolution of the coronal magnetic structure through the solar cycle

Solar Cycle	Coronal Holes*	Current Sheet
Ascending phase	polar holes shrank and disappeared to evolve in a very different way disappeared at different times	the latitudinal extent of the current sheet increases to higher latitudes, disrupting the simple equatorial configuration of the previous minimum
Maximum	no polar holes, but small holes at all latitudes	very complex structure the neutral current sheet extents almost from pole to pole and at mid latitudes small isolated current sheets appear
Descending phase	after the reversal in polarity polar holes reappeared and grow in size with larger equatorial extensions	the structure is simpler and the current sheet has a sinusoidal shape extended over a large range of latitudes
Minimum	polar holes have maximum extensions and there are no equatorial holes	the current sheet is very stable lying over the solar equator

* Based on the description by *Hundhausen et al.* [1981]
† Based on the description by *Hoeksema* [1986].

Table 3. Types of interplanetary shock waves observed by the five spacecraft based on the analysis of the maps of large-scale features.

	no. of Solar Rotations*	Corotating Forward	Corotating Reverse	Transient Forward	Transient Reverse	Percentage of Trans.-Shocks‡
Voyager 1	19**	17	13	21	0	40%
Voyager 2	19	14	10	26	3	55%
Ulysses	18	20†	16	31	3	49%
Pioneer 10	22	25	23	21	?	49%
Pioneer 11	22	42	38	9	1	11%

*for each map of large-scale features (figures 3,4,5,6 and 7).

**data gap for four solar rotations

†four interaction regions were preceded by two forward shocks

‡over the total number of shock waves

Table 4. Averaged parameters of solar wind dynamics as observed by the five spacecraft (proton density data have been normalized to 1 AU using an r^2 dependence).

	<Bulk Speed>* $[km\,s^{-1}]$	<Flux Density>* $[10^8 cm^{-2}s^{-1}]$	Dynamic Pressure* [nPa]	Rate of† Shocks	Rate of† CIRs
Voyager 1	414 ± 70	3.6 ± 3.3	1.75 ± 2.4	3.3	1.2
Voyager 2	426 ± 67	3.6 ± 3.1	2.1 ± 2.3	2.8	0.8
Ulysses	451 ± 81	3.3 ± 3.8	2.6 ± 3.1	3.9	1.0
Pioneer 10	431 ± 81	3.5 ± 2.5	1.8 ± 1.9	3,2	1.0
Pioneer 11	476 ± 96	3.6 ± 3.2	2.0 ± 2.4	4.1	2.3

*average on the whole trajectory

†per solar rotation (27 days).

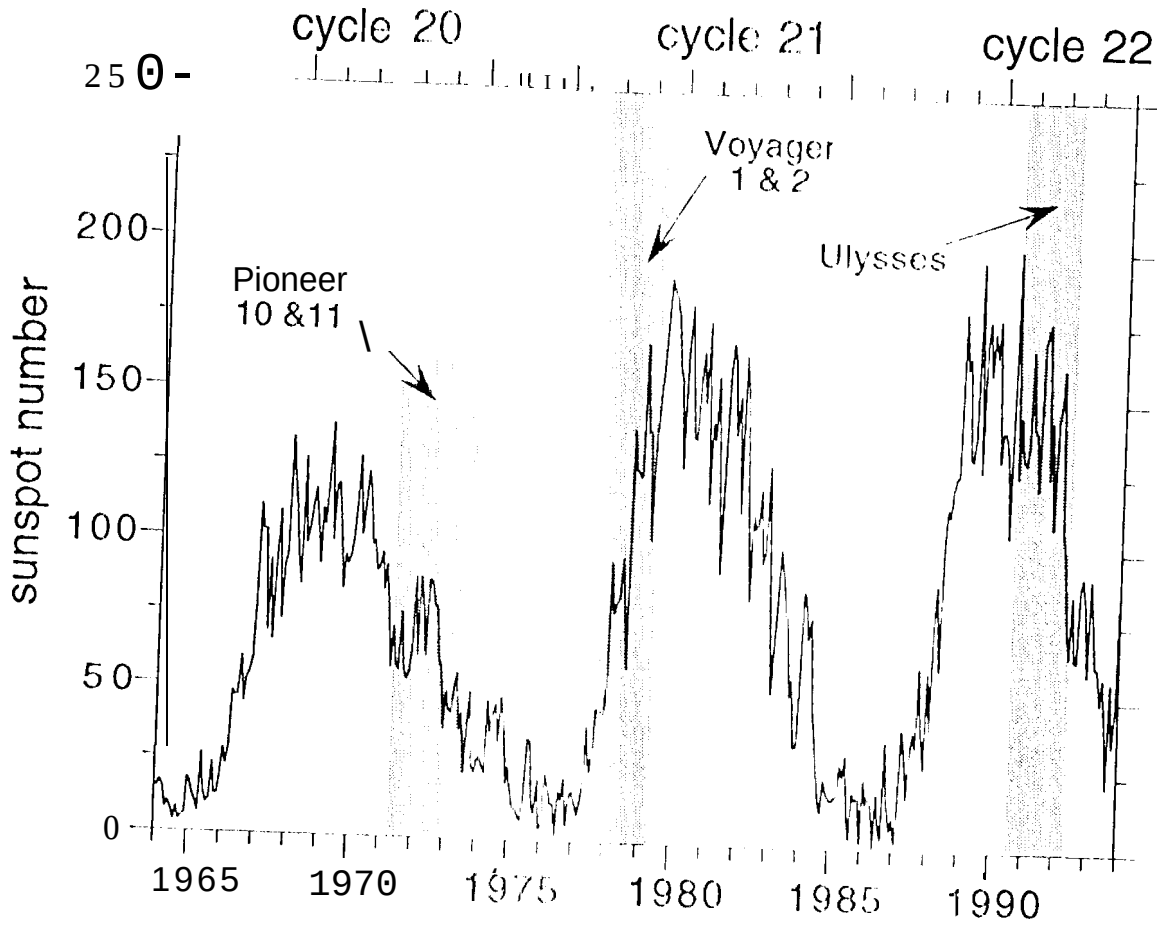
cycle 20
cycle 21
cycle 22
250
200
150
100
50
0
sunspot number
Pioneer
10 &11
Voyager
1 & 2
Ulysses
1965
1970
1975
1980
1985
1990

figure 1

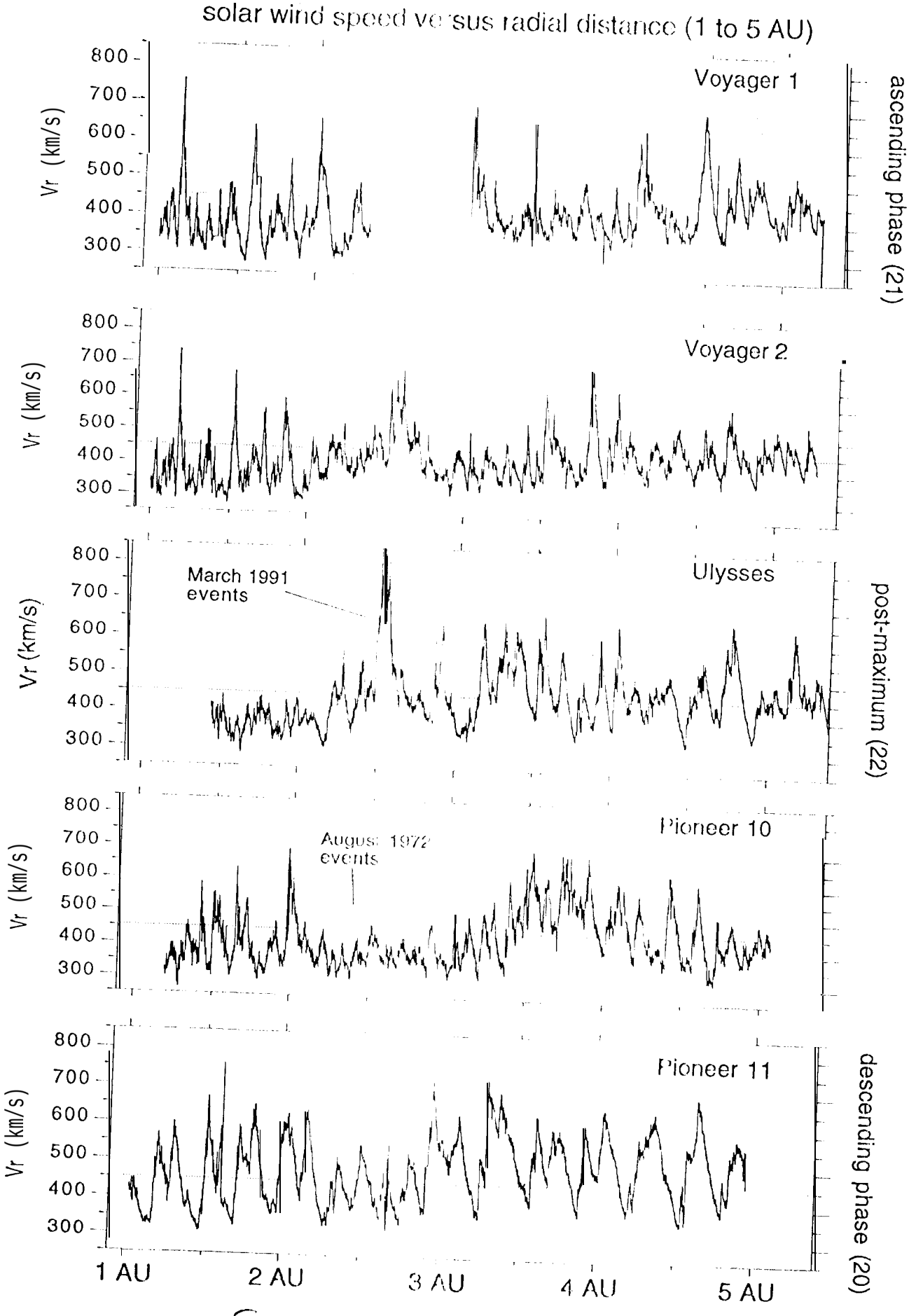
solar wind speed versus radial distance (1 to 5 AU)
Voyager 1
ascending phase (21)
Voyager 2
March 1991
events
Ulysses
post-maximum (22)
August 1972
events
Pioneer 10
Pioneer 11
descending phase (20)
Vr (km/s)
800
700
600
500
400
300
1 AU
2 AU
3 AU
4 AU
5 AU

Figure 2

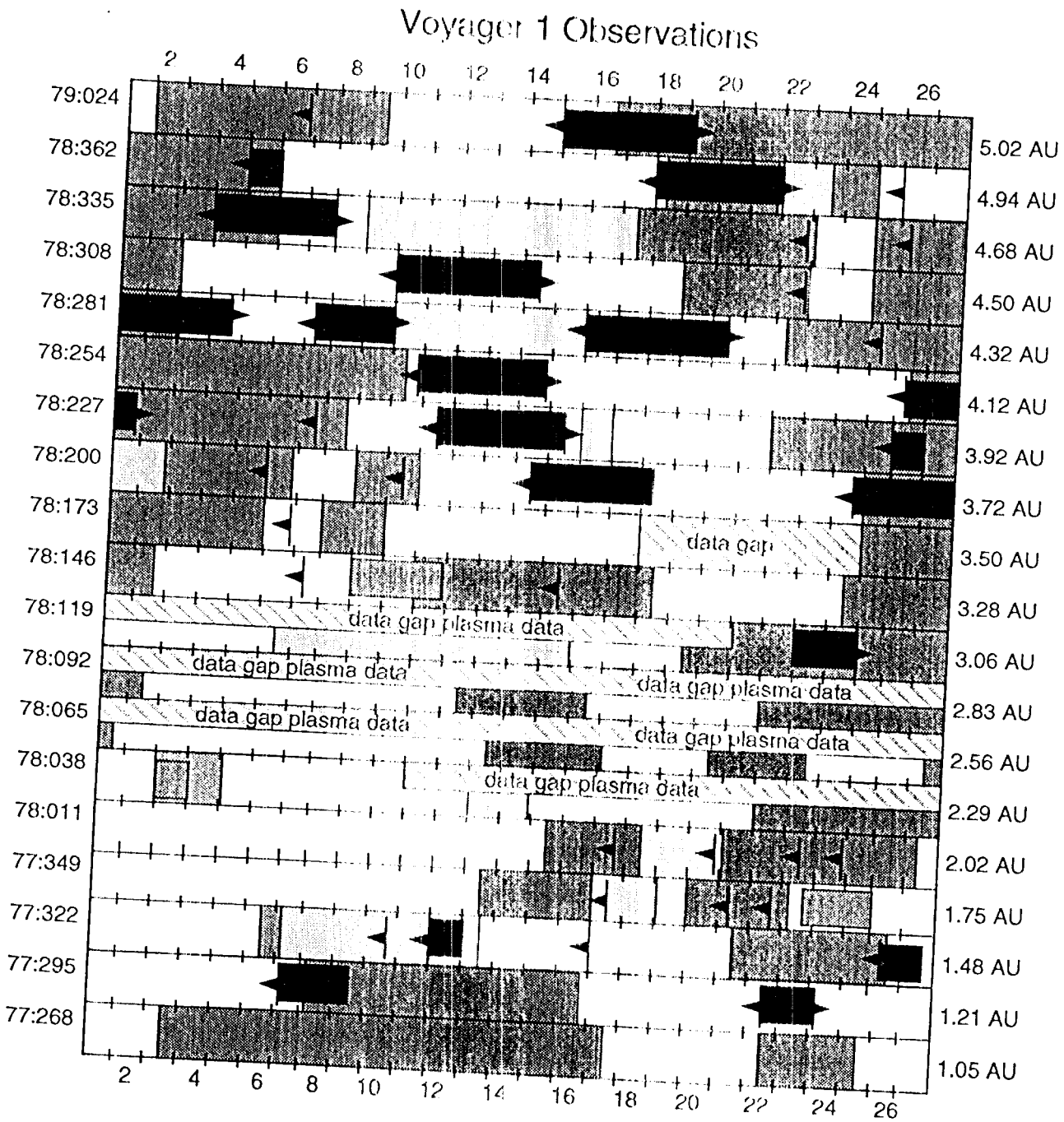
Voyager 1 Observations
2 4 6 8 10 12 14 16 18 20 22 24 26
79:024
78:362
78:335
78:308
78:281
78:254
78:227
78:200
78:173
78:146
78:119
78:092
78:065
78:038
78:011
77:349
77:322
77:295
77:268
5.02 AU
4.94 AU
4.68 AU
4.50 AU
4.32 AU
4.12 AU
3.92 AU
3.72 AU
3.50 AU
3.28 AU
3.06 AU
2.83 AU
2.56 AU
2.29 AU
2.02 AU
1.75 AU
1.48 AU
1.21 AU
1.05 AU
data gap
data gap plasma data
data gap plasma data
data gap plasma data
data gap plasma data
data gap plasma data
2 4 6 8 10 12 14 16 18 20 22 24 26

Figure 3

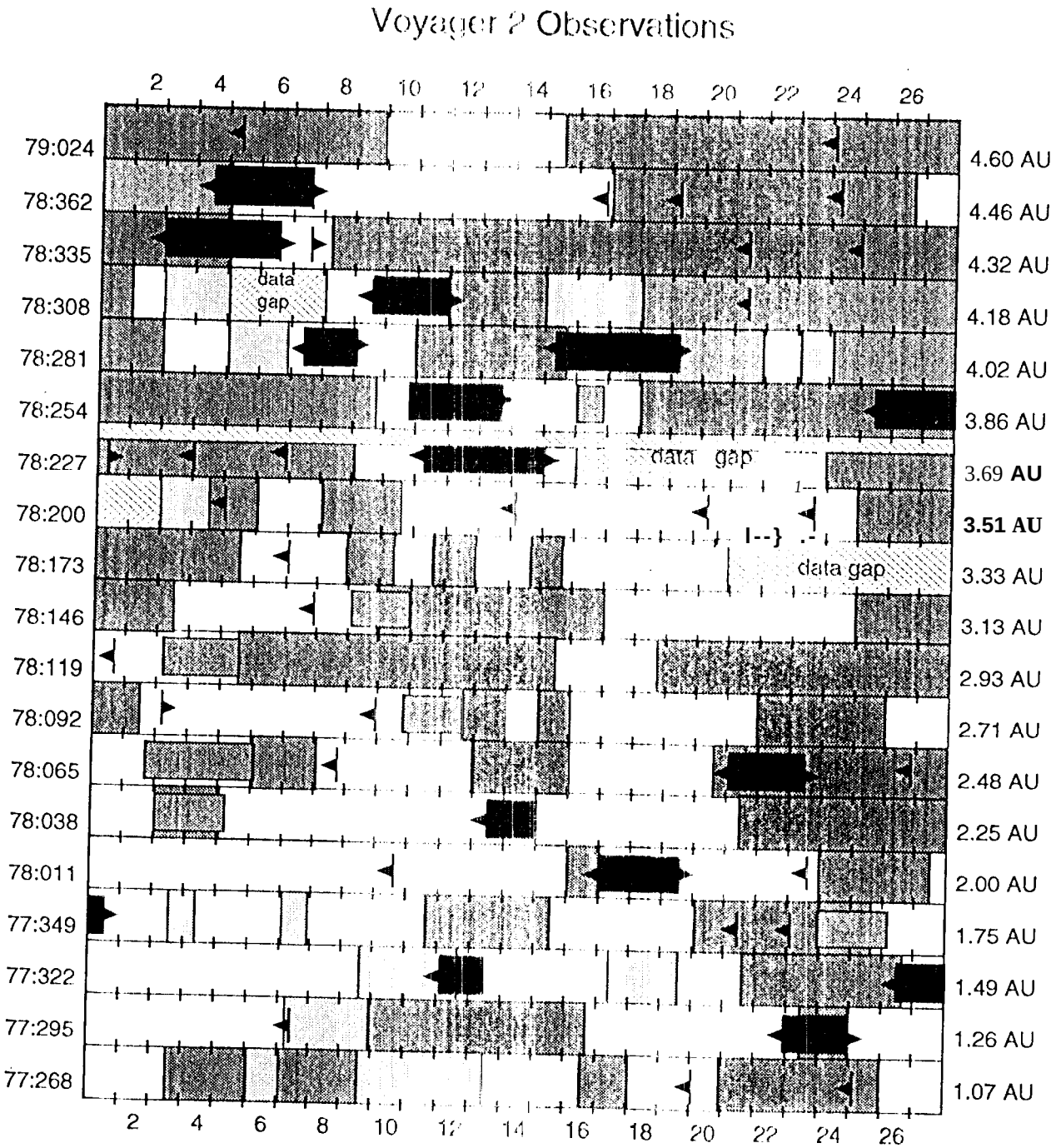
Voyager 2 Observations
2 4 6 8 10 12 14 16 18 20 22 24 26
79:024
78:362
78:335
78:308
78:281
78:254
78:227
78:200
78:173
78:146
78:119
78:092
78:065
78:038
78:011
77:349
77:322
77:295
77:268
4.60 AU
4.46 AU
4.32 AU
4.18 AU
4.02 AU
3.86 AU
3.69 AU
3.51 AU
3.33 AU
3.13 AU
2.93 AU
2.71 AU
2.48 AU
2.25 AU
2.00 AU
1.75 AU
1.49 AU
1.26 AU
1.07 AU
data gap
data gap
data gap
2 4 6 8 10 12 14 16 18 20 22 24 26

Figure 4

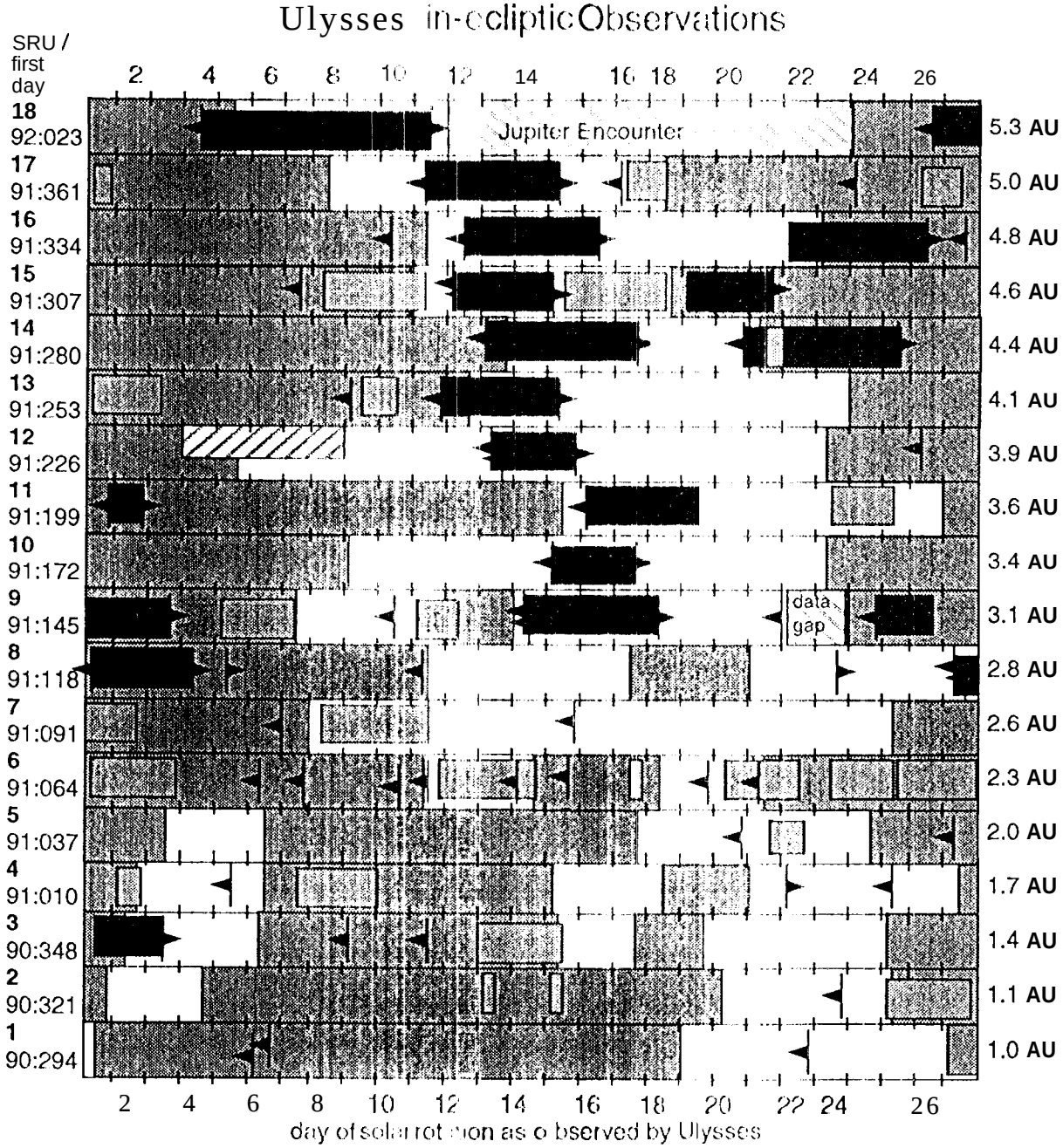
Ulysses in-ecliptic Observations
SRU / first day
2 4 6 8 10 12 14 16 18 20 22 24 26
18 92:023
17 91:361
16 91:334
15 91:307
14 91:280
13 91:253
12 91:226
11 91:199
10 91:172
9 91:145
8 91:118
7 91:091
6 91:064
5 91:037
4 91:010
3 90:348
2 90:321
1 90:294
Jupiter Encounter
data gap
5.3 AU
5.0 AU
4.8 AU
4.6 AU
4.4 AU
4.1 AU
3.9 AU
3.6 AU
3.4 AU
3.1 AU
2.8 AU
2.6 AU
2.3 AU
2.0 AU
1.7 AU
1.4 AU
1.1 AU
1.0 AU
2 4 6 8 10 12 14 16 18 20 22 24 26
day of solar rotation as observed by Ulysses

Figure 5

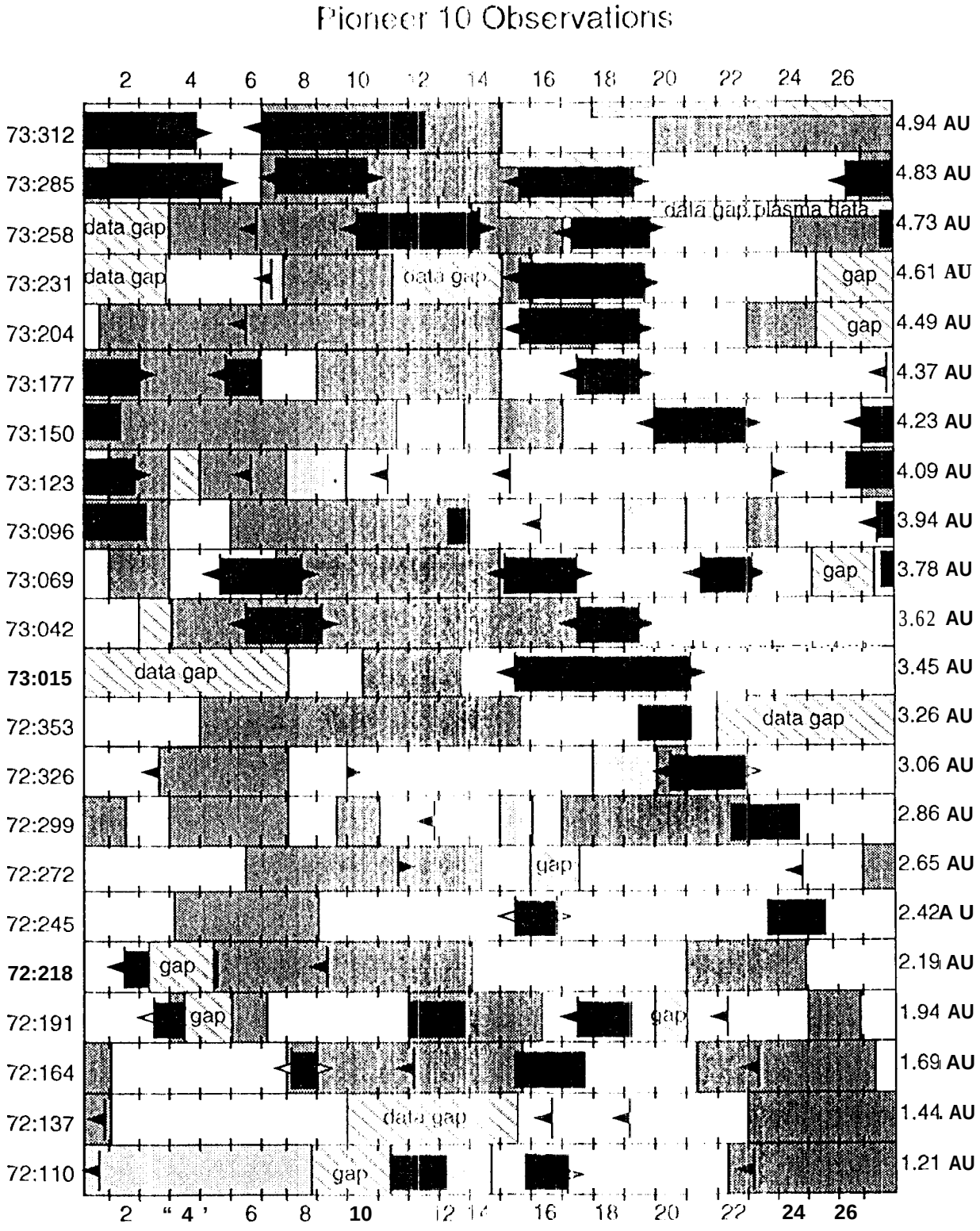
Pioneer 10 Observations
2 4 6 8 10 12 14 16 18 20 22 24 26
73:312
73:285
73:258
73:231
73:204
73:177
73:150
73:123
73:096
73:069
73:042
73:015
72:353
72:326
72:299
72:272
72:245
72:218
72:191
72:164
72:137
72:110
4.94 AU
4.83 AU
4.73 AU
4.61 AU
4.49 AU
4.37 AU
4.23 AU
4.09 AU
3.94 AU
3.78 AU
3.62 AU
3.45 AU
3.26 AU
3.06 AU
2.86 AU
2.65 AU
2.42A U
2.19 AU
1.94 AU
1.69 AU
1.44 AU
1.21 AU
data gap
data gap plasma data
data gap
data gap
gap
gap
gap
data gap
data gap
gap
gap
gap
gap
data gap
gap
2 4 6 8 10 12 14 16 18 20 22 24 26

figure 6

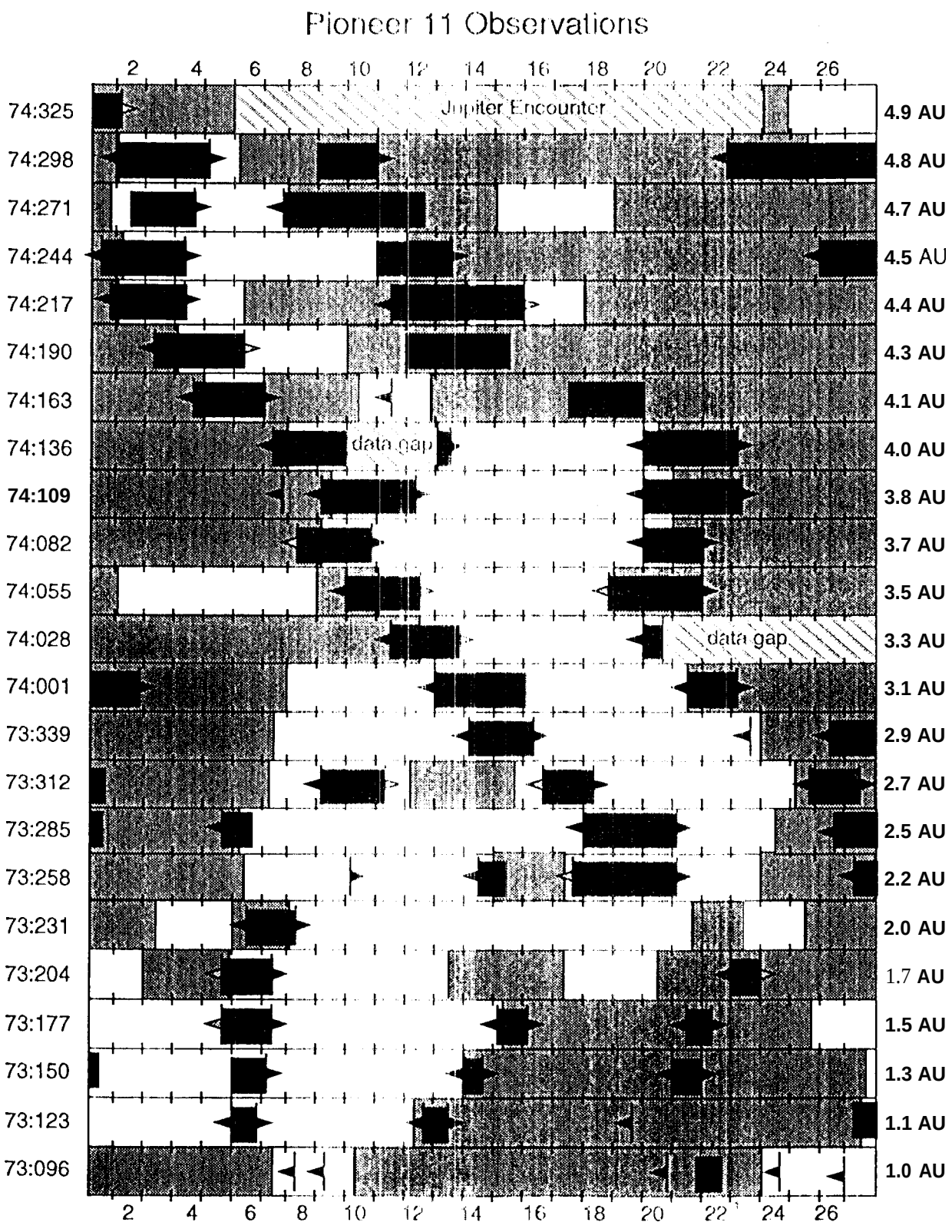
Pioneer 11 Observations
2
4
6
8
10
12
14
16
18
20
22
24
26
Jupiter Encounter
data gap
data gap
74:325
74:298
74:271
74:244
74:217
74:190
74:163
74:136
74:109
74:082
74:055
74:028
74:001
73:339
73:312
73:285
73:258
73:231
73:204
73:177
73:150
73:123
73:096
4.9 AU
4.8 AU
4.7 AU
4.5 AU
4.4 AU
4.3 AU
4.1 AU
4.0 AU
3.8 AU
3.7 AU
3.5 AU
3.3 AU
3.1 AU
2.9 AU
2.7 AU
2.5 AU
2.2 AU
2.0 AU
1.7 AU
1.5 AU
1.3 AU
1.1 AU
1.0 AU

Figure 7

Voyager 1

Voyager 1

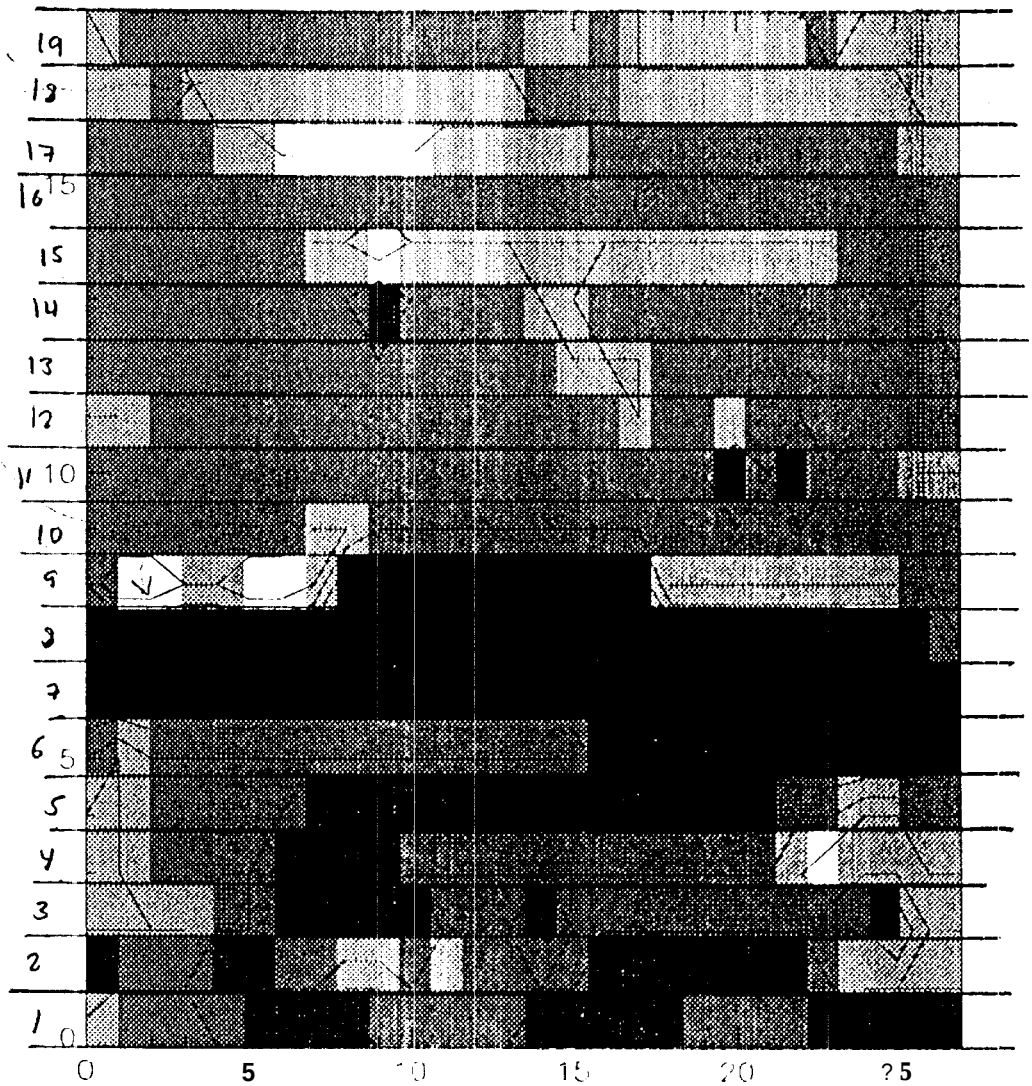

Figure 8a

Voyager 2

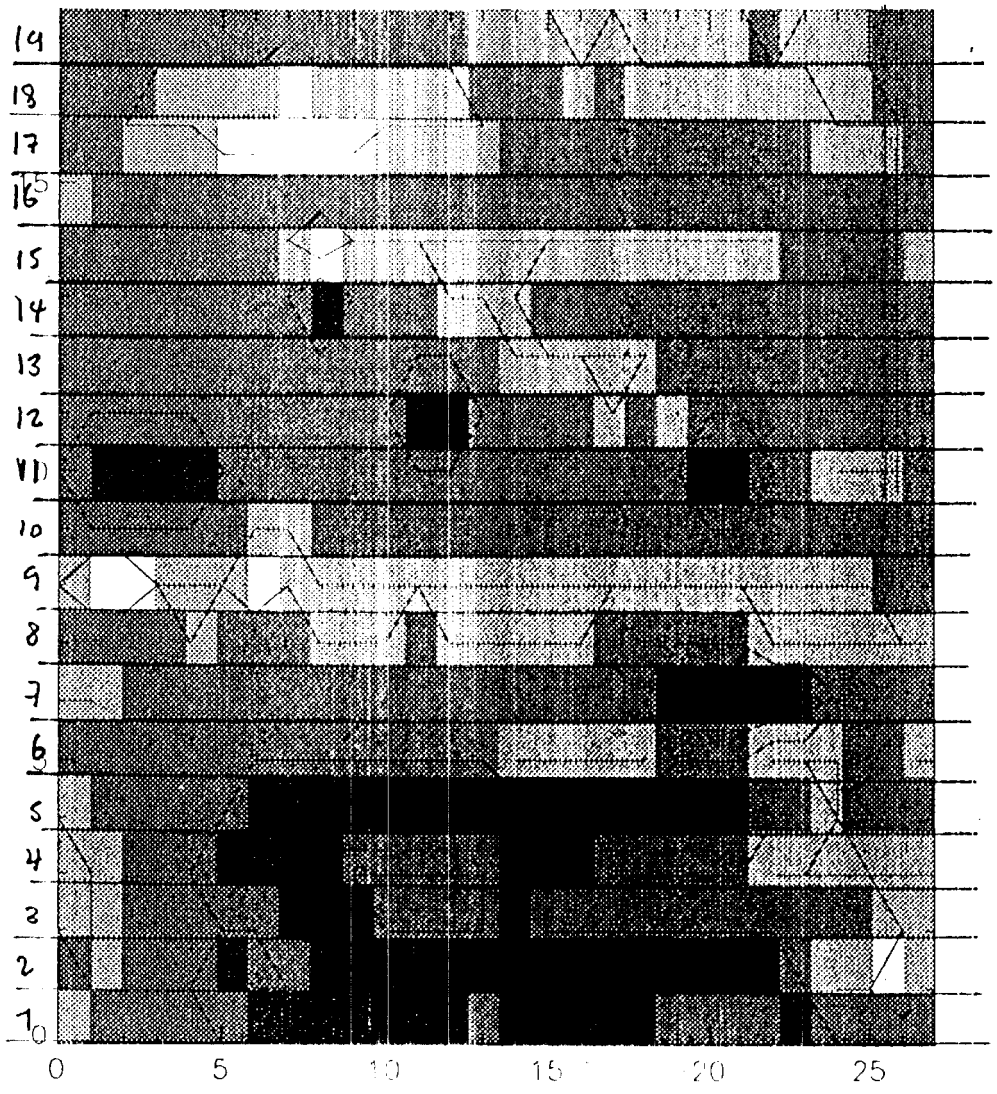

Figure 8b

Pioneer 10

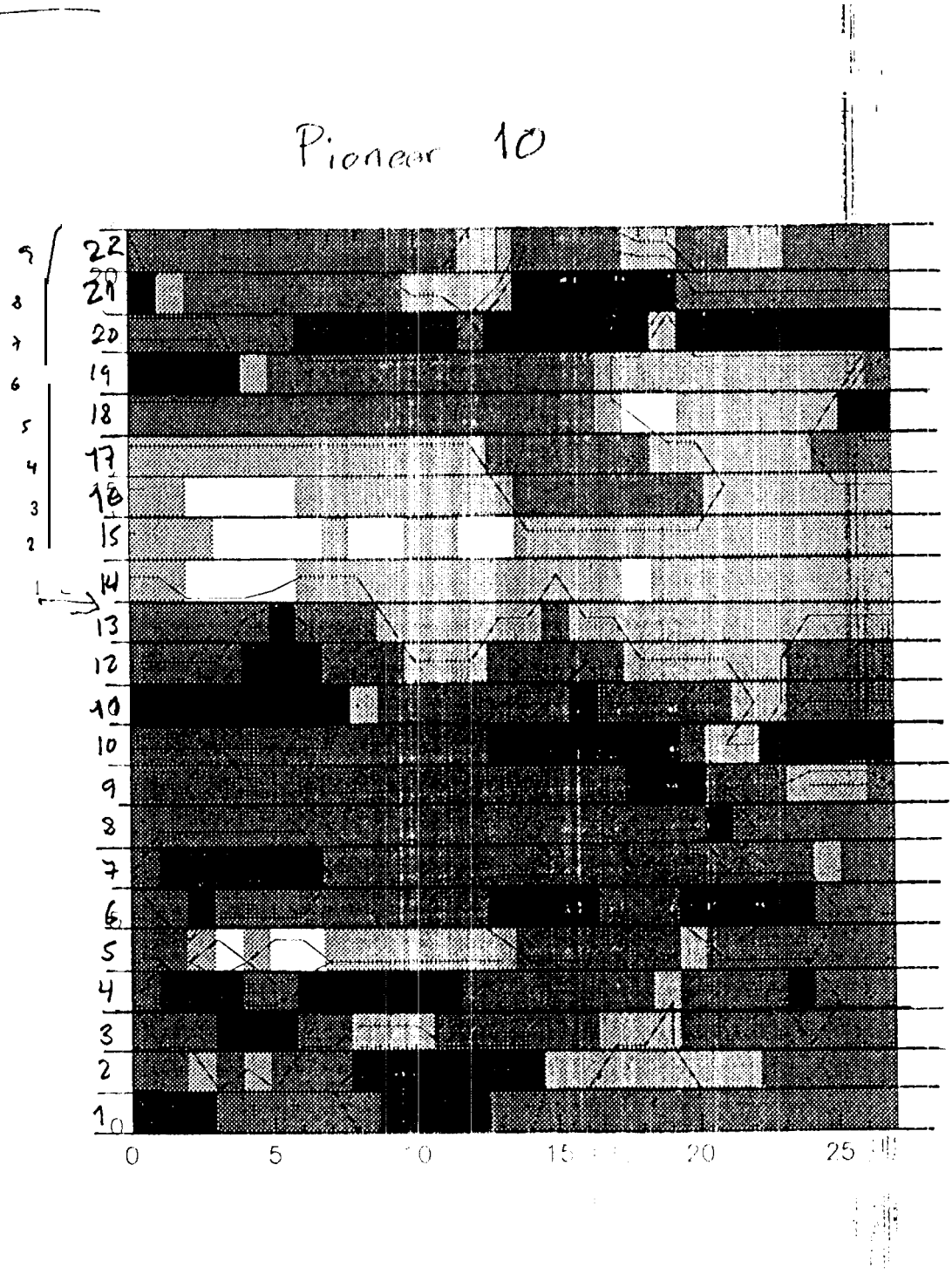

figure 8d

Pioneer 11

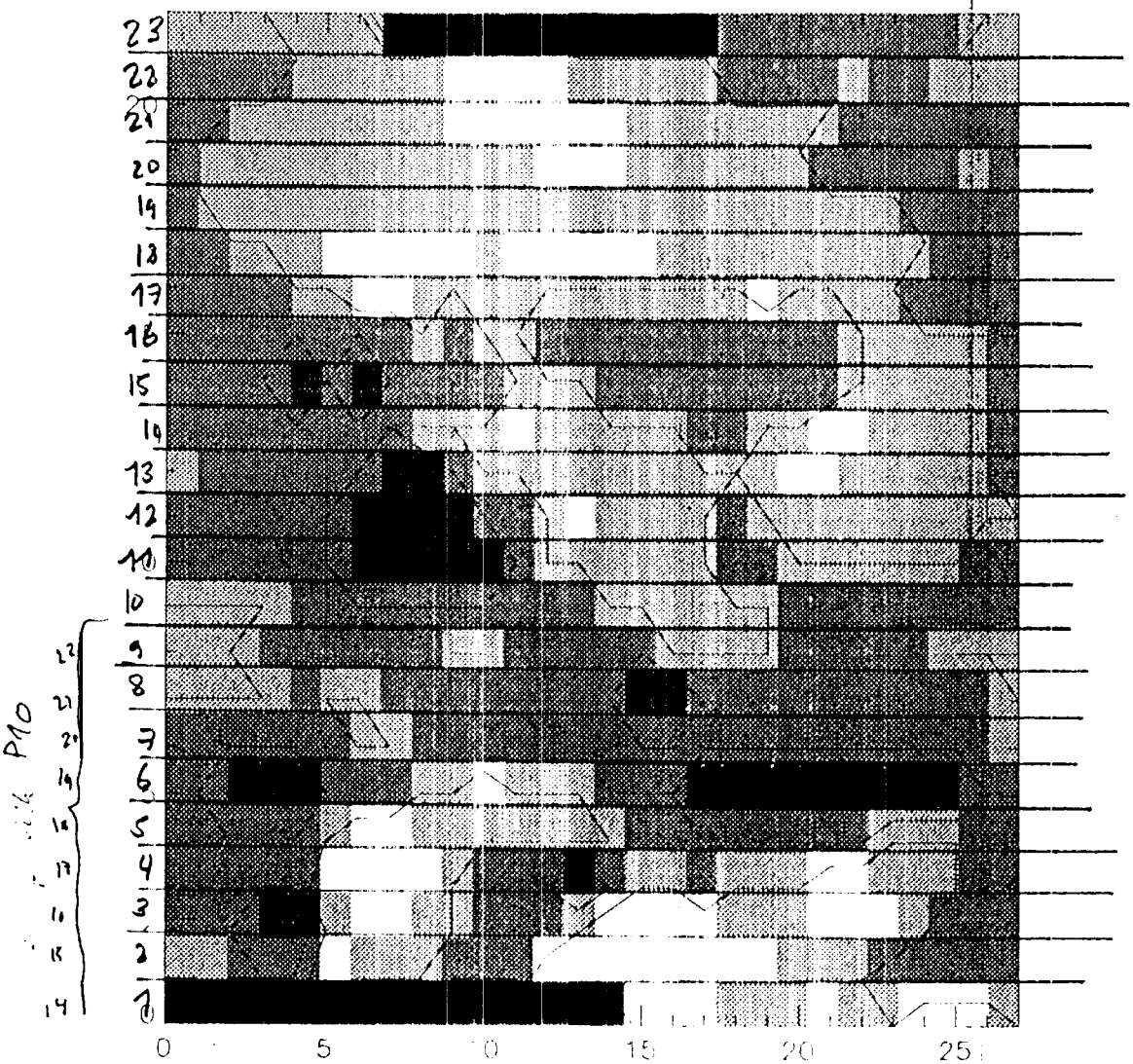

figure 8e

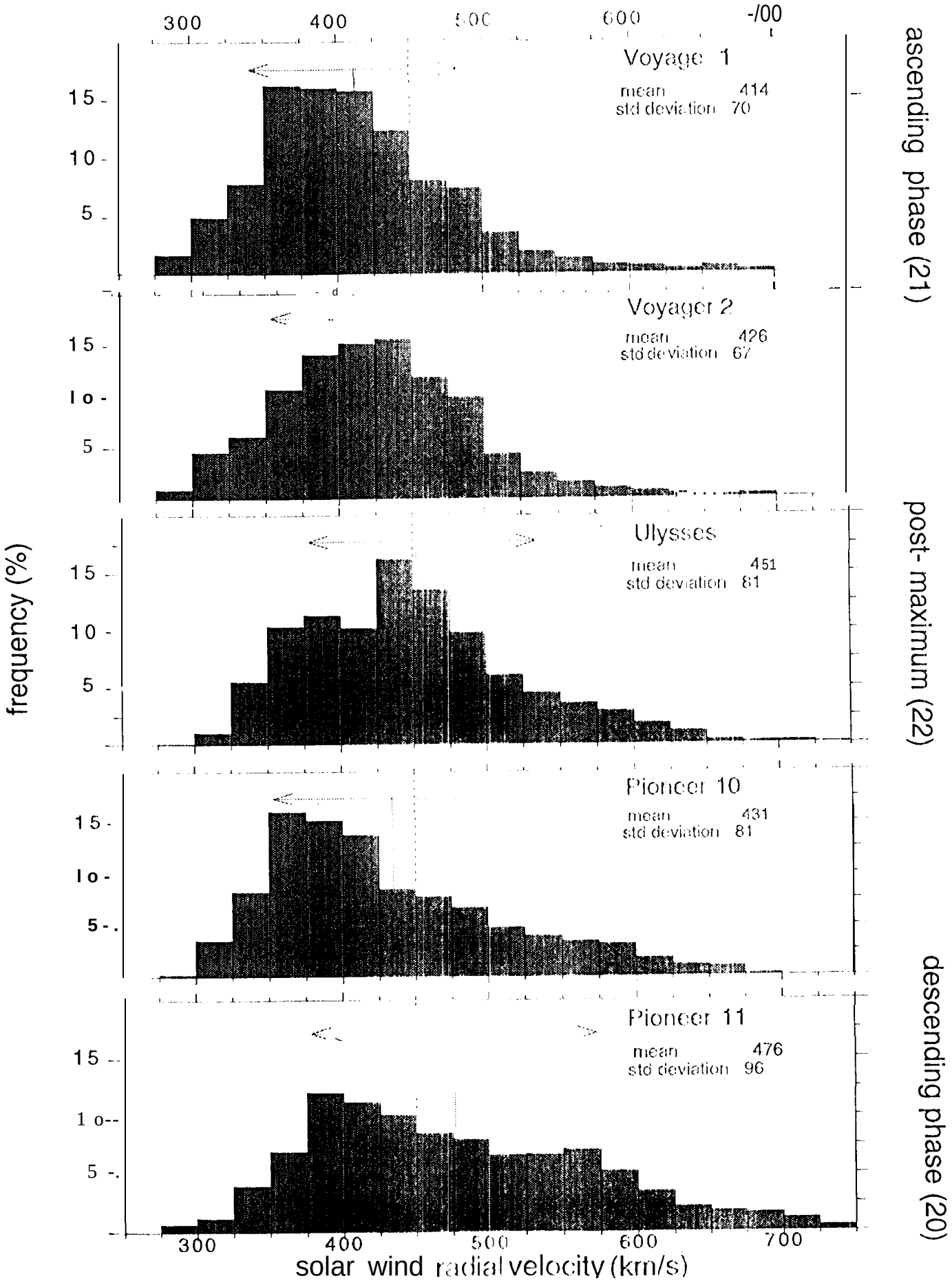
Voyage 1
mean 414
std deviation 70
Voyager 2
mean 426
std deviation 67
Ulysses
mean 451
std deviation 81
Pioneer 10
mean 431
std deviation 81
Pioneer 11
mean 476
std deviation 96
frequency (%)
solar wind radial velocity (km/s)
ascending phase (21)
post- maximum (22)
descending phase (20)

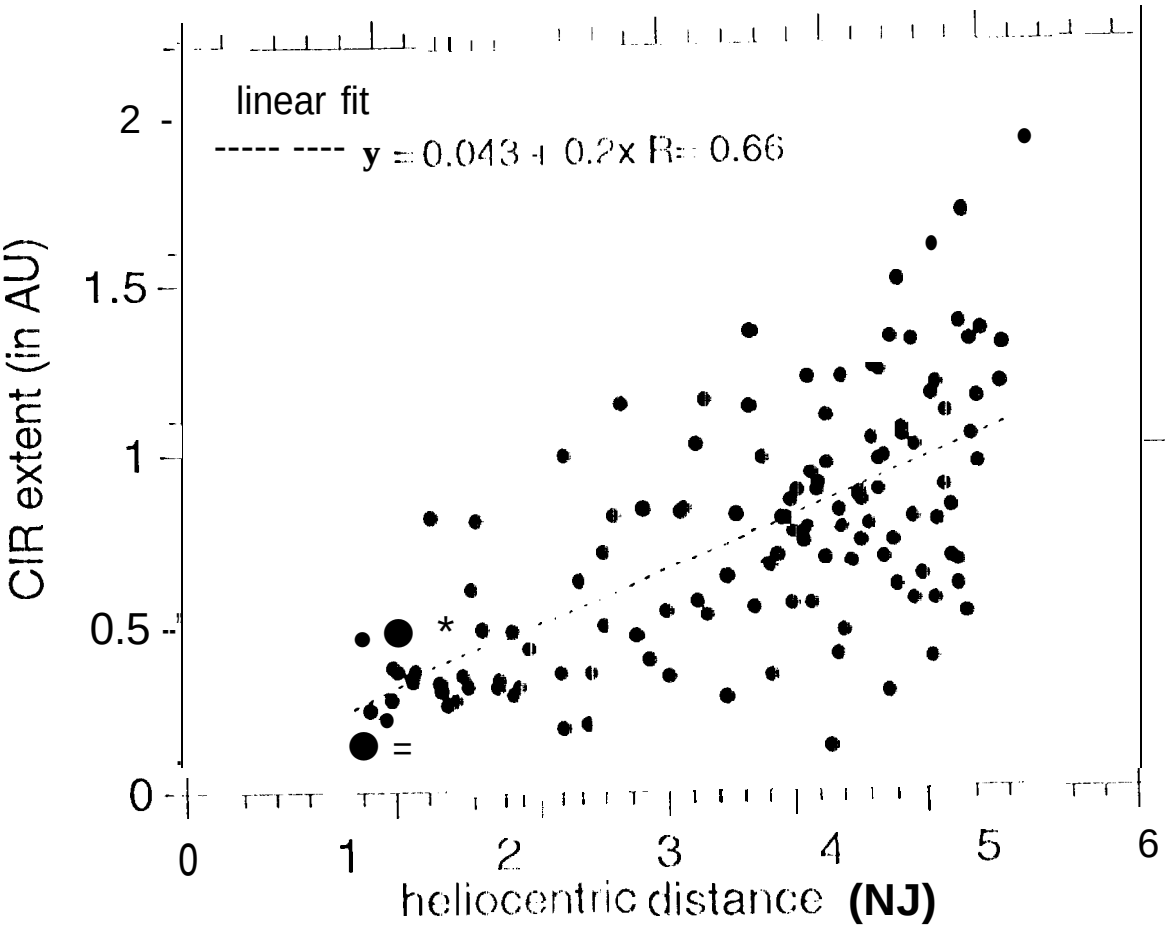
linear fit
----- ---- y = 0.043 + 0.2x R= 0.66
CIR extent (in AU)
heliocentric distance (NJ)
0
0.5
1
1.5
2
0
1
2
3
4
5
6

Figure 10